Compressible Boundary Layer flow on Flat Plate with Different Boundary Conditions

Yugansha Kabra[1], Dr. Vivek K. Sharma[2]

PhD Scholar, Professor

Faculty of Engineering and Technology, Jagannath University, Sitapura Campus, Jaipur (Rajasthan);

Abstract: The Blasius boundary layer is a classical solution for the laminar flow over an isothermal flat plate. It provides an analytical expression for the velocity and temperature profiles within the boundary layer. The resulting compressible Blasius solution would provide expressions for the velocity, density, pressure, and temperature profiles within the compressible boundary layer. However, it's worth noting that obtaining an analytical solution for the compressible case is generally much more challenging compared to the incompressible case. The concept proposed used power law model and Sutherland's viscosity model. The power law model uses a simple mathematical equation to relate shear stress and shear rate, which facilitates calculations and model implementation. The equation is of the form $\tau = K * \gamma^n$, where τ is the shear stress, γ is the shear rate, K is the consistency index, and n is the flow behavior index. Sutherland's viscosity model allows for the extrapolation of viscosity data beyond the range of experimental measurements. This makes it particularly useful when dealing with extreme temperatures or when experimental data is limited. Proper treatment of boundary conditions is crucial in fluid dynamics simulations. The Runge-Kutta method requires appropriate handling of boundary conditions to ensure that the flow variables satisfy the prescribed conditions at the domain boundaries. The method also has limitations in terms of stability, accuracy, and computational cost, which need to be considered when selecting the appropriate numerical scheme. The overall mixed approach provides more accurate calculations related to fluid dynamics.

Keywords- Fluid Dynamics, Sutherland's viscosity model , Runge-Kutta method , Blasius boundary layer , laminar flow

I. INTRODUCTION

Stagnation point flow is the movement of a fluid near the stagnation point or the line. It is also known as potential flow, inviscid flow, or simply stagnation point flow. The flow is specifically designed to funnel in the most effective manner possible. When a streamline comes in, it gets split up and directed outwards in a different direction by separatrices. [1]

Careful consideration is given to these saddle points where a streamline can get deflected if it meets a solid surface. The flow near these stagnation points can then generally be described with potential flow theory, with the exception that viscous effects need to be included when the stagnation point lies on a solid surface. [1]

A theoretical model of particle trapping in a microfluidic device can be described as an incompressible two-dimensional flow in which the velocity is linear in position. [2]

The consistency of this equation is what differentiates the three flow types: extensional, shear, and rotational flows. As the rate of extension throughout the flow is assumed to remain constant, extensional flows are layers of flow moving in or away from each other. The opposite magnitudes of adjacent flows will generate shear flows when there is a concentric field with a non-zero rotational magnitude. Two types of microfluidic stagnation point flows can be combined to provide a convenient way to address different types. From a mathematical perspective, these flows can be described in 2-D as: [2]

$$u_i = a_i x_i \qquad (1)$$

where, a stagnation point flow can be considered to have constant components in the velocity gradient tensor ai, where xi denotes the position vector and ai denotes the velocity gradient tensor with constant components.

$$a_i = \beta \begin{pmatrix} (1+\lambda) & (1-\lambda) \\ -(1-\lambda) & -(1+\lambda) \end{pmatrix} \quad (2)$$

where, "$\beta > 0$ is half the magnitude of the local velocity gradient and λ is a parameter that determines the flow-type. Typically, λ varies from -1 to 1, which indicates a variation from a purely rotational flow ($\lambda = -1$) to a purely extensional flow ($\lambda = 1$)". A shear flow is a superposition of extension and rotation flows, and is considered to be a simple shear flow halfway through. The ratio of vorticity to strain rate is $(1 - \lambda)/(1 + \lambda)$. Thus, it is deduced from their streamline that vortices are maximum in rotational flows, while strain rate is maximum in pure extensional flows. [3]

"From eqn (1) and (2), the velocity components of the flow is given by:25

$$u1 = \beta(x1(1 + \lambda) + x2(1 - \lambda)) \quad (3)$$

$$u2 = -\beta(x1(1 - \lambda) - x2(1 + \lambda)) \quad (4)$$

This gives rise to the family of streamlines described by:

$$Z = (x1 + x2)2 - \lambda(x1 - x2)2 \quad (5)"$$

Equation (5) is clearly the basis for these types of flow, and provides a method for observing them in their theoretical forms. This review examines applications of stagnation points inherent in their structures, with a special emphasis on stagnation point flow generation devices.[3]

II. LITERATURE REVIEW

Arai, F., et al. 2001 , This system works by restricting the size of area in which cells or microbes are present to only a small region just after they exit the sample chamber. This way, when cells flow into the extraction port with high speed, they are forced to come out through the narrow space between two adjacent microchannels. The target is transported using laser manipulation from the sample chamber and placed on this small region before it can be taken out at a high speed through an extraction port. When you're trying to manipulate cells so that they can be transferred, it's important for them to be exposed to a stable level of forces. Therefore, once in this environment, authors proposed that pressure within this particular region should be carefully adjusted to make sure that there is always an even distribution of forces on both sides of the cell during transport. [4]

Sin, V. K., & Tong, T. Y., 2008 investigated the numerical simulation of two-dimensional stagnation point flow with STAR-CD CFD software and found that simulations were in good agreement with Star's similarity solutions for high aspect ratios in the stagnation point region. As a result, numerical simulation of nonzero vorticity yields the conclusion that boundary layer thickness remains constant at the stagnation point region where vorticity generated near a wall is prevented from diffusing far away by convection towards the wall. There is no longer a balance between diffusion and convection of vorticity in regions far from the stagnation point, which results in a decrease in boundary layer thickness along walls. [5]

Sin, V. K., & Chio, C. K., 2011 , solved the Navier-Stokes equations in two dimensions with STAR-CD computational fluid dynamics (CFD) software and compared the results with

similarity asymptotic solutions of the full Navier-Stokes equations. For four different aspect ratios, velocity distribution was examined both in the inner region near the wall, as well as in the outer region away from the wall. [6]

Kazem, S. , et al. 2011, authors investigate the advantages of radial basis function when it comes to solving nonlinear equations governing energy and momentum in steady laminar flow through porous media filled with an incompressible, viscous conducting fluid. The flow is directed towards a permeable stretching surface where heat transfer takes place. Variations of porosity, surface stretching velocity, and heat emission/absorption coefficient have a pronounced effect on both flow and thermal transfer. To simplify the process of finding a solution over most of the domain $(0..\infty)$, authors utilize collocation points in conjunction with Gaussian radial basis function to satisfy the boundary condition at infinity. [7]

Zhu, X. D. , et al. 2014, This paper presents an analytical investigation of viscous flow of a micropolar fluid in the vicinity of an axisymmetric stagnation point on a shrinking porous cylinder using homotopy analysis method. An appropriate similarity transformation is used to convert the governing nonlinear partial differential equations into a system of ordinary differential equations. Graphical presentations of the serious solutions are provided and recurrence formulae for finding the relevant coefficients are given. The effects of varying parameters on this problem have been studied and our attempt to find a solution via homotopy analysis is in agreement with numerical results. [8]

Borrelli, A., et al. 2015 , A precise solution for the steady plane magnetohydrodynamics oblique stagnation-point flow of an homogeneous, conductive micropolar liquid over a motionless uncharged dielectric in the presence of a non-uniform external magnetic field and uniform external electric field is attained. Through utilizing similarity transformations which modify the geometric restrictions and parameters just enough to make differentials into derivatives on our intended function, the issue is converted into a non-linear ordinary

differential boundary value problem. The impact of magnetic fields on both velocity profiles and microrotation profiles are illustrated graphically along with discussion. [9]

Brykina, I. G., 2015, The simple analytical solutions for heat flux normalized by the value at a stagnation point are obtained for three dimensional (3D) hypersonic flows over blunt bodies at moderate and high Reynolds numbers. As a result of comparing with numerical solutions, this type of formula can be used to predict the heat transfer on blunt surfaces exposed to chemically reacting gas flows in 2D and 3D. [10]

Roşca, N. C., & Pop, I. , 2015 , In their study "The Mixed Convection Boundary-Layer Flow near the Loauthorsr Stagnation Point of a Horizontal Circular Cylinder with a Second-Order Slip Velocity Model and a Constant Surface Heat Flux," Roşca, et al. investigate how different heights on the cylinder change the flow patterns. By choosing appropriate similarity variables, they can see which parts of the pattern are similar enough to each other that they can be simplified into one variable. They then solved the system numerically for different values of height and found two pattern branches: an upper branch that is stable and physically realizable, and a loauthorsr branch that is unstable. [11]

Haq, R. U., et al. 2015 , According to a new model, natural convective micropolar fluid flowing around an elongated sheet of metal heated on one side will bend over the heated surface much faster than the boundary between it and the ambient fluid just outside. This is because radiation converts kinetic into thermal energy more efficiently near a heated surface – and the hotter, more buoyant gas bends more quickly than the slower-moving ambient gas. This process also creates eddies that mix with water vapor in a process called condensation, which creates nanoparticles. The model generates heat transfer rates accurate to within 10% for nanofluid flow in curved channels. [12]

Soid, S. K. , et al. 2015 , studied unsteady magnetohydrodynamic (MHD) stagnation point flow over a stretching/shrinking sheet in this paper. These problems were transformed into an

ordinary differential equation by using the proper variables. Solving the analogy differential equation might lead to dual solutions for different parameter values and the results can be seen in a table as well as four figures for every value of parameters. [13]

Ibrahim, W. N. A. , 2015 , This paper examines the influence of a magnetic field and convective boundary condition upon MHD stagnation-point flow with heat transfer due to nanofluid, incorporating Brownian motion and thermophoresis variables. By employing a similarity transformation, the corresponding non-linear governing equations and complementary boundary conditions are derived in a dimensionless form. Numerical solutions of the equations are developed using fourth-order Runge-Kutta method together with shooting technique. It is seen that the resultant expressions depend on M, B, Bi, Pr, Le, Nb, Nt, Rc and A. Results comprise velocity and temperature profiles as well as skin friction coefficient, local Nusselt number (Nu') and Sherwood number (St). It is established that velocity and skin friction coefficient on stretching sheet are greatly impacted by velocity ratio (B <; 1) and magnetic parameters. [14]

Ibrahim, W. N. A., 2017 , This paper examines a mathematical model for effective heat protection on hypersonic aircraft side surfaces and spherical nozzle surfaces. It is determined that a unique control restoration is viable in the stagnation point in one-dimensional scenarios, wherein monotonous dependence of heat and mass transfer parameters on controls is exhibited. In two-dimensional cases, conditions of diffeomorphism for control pairs and local heat and mass transfer pairs are proved. Experimental results revealed domains with "heat-friction" values ranging from 90% to 97%. [15]

Subrahmanyam, P. B., et al. 2018, A group of researchers conducted an extensive parametric study on a variety of parameters, including Reynolds numbers up to 20000. The study explored how the use of a tapered micro nozzle, rather than a traditional one, can produce varying cooling effects for different spaces and contexts. It was found that for high-

powered packages with tapered nozzles, the use of a higher-Reynolds number in conjunction with more distance from the nozzle to the package reduces surface temperatures 10 degrees Celsius - 20 degrees Celsius. The study also investigated surface Nusselt number and heat transfer coefficient. A k-θ model was used to predict turbulent flow and its associated characteristics. Moving forward, it is important to be able to design robust systems that can effectively handle higher power densities using current methods in direct on-die impingement cooling. [16]

Ali, F., & Zaib, A., 2019, In this article, the authors examined how the velocity and temperature of a nanoparticle-laden Eyring-Poauthorsll nanofluid varies as it moves between two surfaces. To do so, they applied the boundary layer governing PDEs, which were converted to non-similar (ODEs) problems with self-similar conversion, in order to calculate their numerical solutions. Furthermore, the authors addressed how physical parameters affect these computed quantities through examining velocity and concentration graphs and the skin friction coefficient of local zones. Finally, the authors examined numerical outcomes of skin friction factor Nusselt and Sherwood number and found that these quantities increased with decreasing values of liquid interface film thickness. [17]

Faizan, M., & Zaib, A. , 2020 , "This research article explores the unsteady flow of Maxauthorsll fluid in the occurrence of nano-liquid over a stretching surface." At first, non-linear system of PDEs were successfully transformed into ODEs using an appropriate transformation and then solved numerically with the shooting scheme. Graphical illustrations and tabular values were utilized to illustrate the influential variables of the flow field, concentration, and temperature distribution profile. The authors found that when Maxauthorsll parameter had large values, the fluid motion exhibited decreasing behavior; however, when the unsteady parameter had increasing values, an opposing trend was observed in

concentration field. Their results were also compared to existing literature which showed tremendous agreement. [18]

Based on the provided information, here's a comparison table summarizing the key aspects of the papers:

Paper	**Year**	**Method/Approach**	**Key Findings**
Arai, F., et al. 2001	2001	Restriction and laser manipulation of cells	Stabilizing forces for cell manipulation through pressure adjustment
Sin, V. K., & Tong, T. Y., 2008	2008	Numerical simulation of stagnation point flow	Agreement with similarity solutions, constant boundary layer thickness near stagnation point
Sin, V. K., & Chio, C. K. 2011	2011	Solving Navier-Stokes equations in 2D	Examined velocity distribution near the wall and in the outer region
Kazem, S., et al. 2011	2011	Radial basis function for solving nonlinear equations	Application in steady laminar flow through porous media filled with a conducting fluid
Zhu, X. D., et al. 2014	2014	Analytical investigation of micropolar fluid flow	Homotopy analysis method, effects of varying parameters studied
Borrelli, A., et al. 2015	2015	Steady magnetohydrodynamics flow of micropolar liquid	Non-linear ordinary differential boundary value problem, graphical representation of velocity and microrotation profiles

Roşca, N. C., & Pop, I. 2015	2015	Heat flux in hypersonic flows over blunt bodies	Simple analytical solutions for heat transfer in 3D hypersonic flows
N. C. Roşca, et al. 2015	2015	Mixed convection boundary-layer flow	Investigation of flow patterns near the Loauthorsr stagnation point of a horizontal circular cylinder
Haq, R. U., et al. 2015	2015	Convective micropolar fluid flow around a heated surface	Rapid bending of fluid over a heated surface, condensation and nanoparticle formation
S. K. Soid, et al. 2015	2015	Unsteady magnetohydrodynamic stagnation point flow	Transformation into ordinary differential equation, dual solutions for different parameter values
Ibrahim, W. N. A., 2015	2015	MHD stagnation-point flow with heat transfer	Magnetic field and convective boundary condition effects on nanofluid flow
Bilchenko, G., & Bilchenko, N. 2017	2017	Heat protection on hypersonic aircraft surfaces	Control restoration, diffeomorphism for control pairs, and local heat and mass transfer pairs
Subrahmanyam, P. B., et al. 2018	2018	Parametric study on cooling effects in micro nozzles	Tapered micro nozzle design, impact of Reynolds number and distance on surface temperatures
Ali, F., & Zaib, A. , 2019	2019	Velocity and temperature of nanoparticle-laden nanofluid	Boundary layer PDEs, self-similar conversion to ODEs, effects of

			physical parameters
Faizan, M., & Zaib, A. , 2020	2020	Unsteady flow of Maxwell fluid with nano-liquid	Transformation of PDEs to ODEs, numerical solutions, influence of flow field and concentration distribution

III. PROPOSED FLOW MODEL

Consider a fluid that flows around a non-orthogonal stagnation point on a flat, fixed plate. On the Cartesian coordinate plane with normal to x-axis and the y-axis being along the plate, this is a flow that only takes place in the positive y direction.

$$\frac{\partial \rho u}{\partial x} + \frac{\partial \rho v}{\partial y} = 0 \quad (1)$$

$$\rho \left(u \frac{\partial u}{\partial x} + v \frac{\partial v}{\partial y}\right) = -\frac{\partial p}{\partial x} + \frac{\partial}{\partial y} \mu \frac{\partial u}{\partial y} \quad (2)$$

$$\rho c_p \left(u \frac{\partial T}{\partial x} + v \frac{\partial T}{\partial y}\right) = -u\frac{\partial p}{\partial x} + \frac{\partial}{\partial y} k \frac{\partial T}{\partial y} + \mu \left(\frac{\partial u}{\partial y}\right)^2 \quad (3)$$

Blassious Boundary Conditions are follows:

$$\frac{\partial \rho u}{\partial x} + \frac{\partial \rho v}{\partial y} = 0$$

u>>>v

and,

$$\frac{\partial}{\partial x} \lll < \frac{\partial}{\partial y} \quad (4)$$

Conservation of y-momentum

$$\frac{\partial P}{\partial y} = 0 \quad (5)$$

$$\rho\left(u\frac{\partial u}{\partial x}+v\frac{\partial v}{\partial y}\right) = \frac{\partial}{\partial y}\mu\frac{\partial u}{\partial y}$$

Conservation of Energy

$$\rho c_p\left(u\frac{\partial T}{\partial x}+v\frac{\partial T}{\partial y}\right) = \frac{\partial}{\partial y}k\frac{\partial T}{\partial y}+\mu\left(\frac{\partial u}{\partial y}\right)^2$$

Where,

$$\frac{T_e}{T}=\frac{\rho}{\rho_e}$$

$$\eta=\frac{u_e}{\sqrt{2\xi}}\int_0^y \rho dy$$

Where ,

$$\xi=\mu_e\rho_e\, u_e\, x$$

$Let\ assume\ that\ the$ stream function is

$$\psi=\sqrt{2\xi}\, f(\eta)$$

The u and v denote velocities which can be evaluated from stream functions as,

$$u=\frac{1}{\rho}\frac{\partial\varphi}{\partial y}$$

$$v=-\frac{1}{\rho}\frac{\partial\varphi}{\partial x}$$

$Now\ , \xi=\mu_e\rho_e\, u_e\, x$

And we have,

$$\eta=\frac{u_e}{\sqrt{2\xi}}\int_0^y \rho dy$$

$$\eta=\frac{u_e y\rho}{\sqrt{2\xi}}$$

$$\eta = \frac{u_e y \rho}{\sqrt{2\mu_e \rho_e \, u_e \, x}}$$

$$\frac{\partial \eta}{\partial y} = \frac{u_e \rho}{\sqrt{2\xi}}$$

$$\frac{\partial \eta}{\partial x} = \frac{u_e y \rho}{\sqrt{2\mu_e \rho_e \, u_e \, x}} - \frac{1}{2} x^{-3/2}$$

$$\frac{\partial \eta}{\partial x} = \frac{-\eta}{2x}$$

$$u = \frac{1}{\rho} \frac{\partial \varphi}{\partial y}$$

$$= \frac{1}{\rho} \frac{\partial \varphi}{\partial y} \frac{\partial \eta}{\partial y}$$

$$= \frac{1}{\rho} \frac{\partial (\sqrt{2\xi} \, f(\eta))}{\partial y}$$

$$= \frac{1}{\rho} \left(\sqrt{2\xi} \, \frac{df}{d\eta} \right) \frac{u_e \rho}{\sqrt{2\xi}}$$

$$u = u_e f'(\eta)$$

$$v = -\frac{1}{\rho} \frac{\partial \varphi}{\partial x}$$

$$= -\frac{1}{\rho} \left[\frac{\partial \psi}{\partial \xi} \frac{\partial \xi}{\partial x} + \frac{\partial \psi}{\partial \eta} \frac{\partial \eta}{\partial x} \right]$$

$$= \frac{-1}{p} \left[\frac{1}{2\sqrt{2\xi}} 2 f(\eta) \, \mu_e \rho_e \, u_e \, x + \left(\sqrt{2\xi} \, f' \right) \left(\frac{-\eta}{2x} \right) \right]$$

$$= \frac{\partial u}{\partial y} = \frac{2u}{2\eta} \frac{\partial \eta}{2y}$$

$$= \frac{u_e^2 \rho f''(\eta)}{\sqrt{2}}$$

$$\frac{\partial}{\partial y} \left(\mu \frac{\partial u}{\partial y} \right) = \frac{\partial}{\partial \eta} \left(\mu \frac{\partial u}{\partial y} \right) \frac{\partial \eta}{\partial y}$$

$$= \frac{\partial}{\partial \eta} \left(\frac{\mu u_e^2 \rho}{\sqrt{2\xi}} f'' \right) \frac{u_e \rho}{\sqrt{2\xi}}$$

$$= \frac{u\rho^2 f'''(\eta) u_e^3}{2\xi}$$

$$\frac{\partial u}{\partial x} = \frac{\partial u}{\partial \eta}\frac{\partial \eta}{\partial x}$$

$$\frac{\partial u}{\partial x} = \frac{\partial\left(u_e f'(\eta)\right)}{\partial \eta}\frac{\partial \eta}{\partial x}$$

$$\frac{\partial u}{\partial x} = u_e f''(\eta)\left(\frac{-\eta}{\partial x}\right)$$

putting values of $u, \frac{\partial u}{\partial x}, v, \frac{\partial v}{\partial x}$ and $\frac{\partial}{\partial y}\left(\mu\frac{\partial u}{\partial y}\right)$ en eqn (2).

$$\frac{\rho\mu}{\rho_e\mu_e} f''' + ff'' = 0.$$

$$\theta = \frac{T - T_\infty}{T_e T_\infty} g(\eta).$$

Nondimensional.

$$\text{Cp}\rho\left(u\frac{\partial T}{\partial x} + v\frac{\partial T}{\partial y}\right) = \frac{\partial}{\partial y}\left(k\frac{\partial T}{\partial y}\right) + \mu\left(\frac{\partial u}{\partial y}\right)^2$$

$$\text{cp}\rho\left(u\frac{\partial \theta}{\partial x} + \frac{v\partial}{\partial y}\right) = \frac{\partial}{\partial y}\left(k\frac{\partial \theta}{\partial y}\right) + \mu\left(\frac{\partial u}{\partial y}\right)^2 - (\hat{4})$$

$$\frac{\partial \theta}{\partial x} = g'(\eta)\frac{\partial \eta}{\partial x}$$

$$= g'(\eta)\left(\frac{-n}{\partial x}\right)$$

$$\frac{\partial \theta}{\partial y} = g'(\eta)\frac{\partial \eta}{\partial y}$$

$$= g'(\eta)\left(\frac{u_e\rho}{\sqrt{2\xi}}\right)$$

$$= \frac{\partial}{\partial y}\left(k\frac{\partial \theta}{\partial y}\right)$$

$$= \frac{\partial}{\partial \eta}\left(kg'(\eta)\frac{u_e\rho}{\sqrt{2\xi}}\right)\frac{\partial \eta}{\partial y}$$

(5)

The compressible Blasius similarity equations are given by:

$$\left(\frac{\rho\mu}{\rho_e\ \mu_e} f''\right)' + ff'' = 0 \tag{6}$$

$$\left(\frac{\rho\mu}{\rho_e\ \mu_e}\ \frac{1}{P_r} g'\right)' + fg' + \frac{u_e^2}{(h_0)_e}\left[\left(1 - \frac{1}{P_r}\right)\frac{\rho\mu}{\rho_e\ \mu_e} f'f''\right]' = 0 \tag{7}$$

Where:

$$\frac{u_e^2}{(h_0)_e} = \frac{u_e^2}{\left(h_e + u_e^2/2\right)} = \frac{1}{\frac{c_p T_e}{u_e^2} + \frac{1}{2}} = \frac{1}{RT_e/(\gamma - 1)u_e^2 + \frac{1}{2}} \tag{8}$$

$$=\frac{1}{1/(\gamma-1)M_e^2+\frac{1}{2}}=\frac{2(\gamma-1)M_e^2}{2+(\gamma-1)M_e^2} \quad (9)$$

Letting,

$$C=\frac{\rho\mu}{\rho_e\ \mu_e} \text{ and } K=\frac{1}{1/(\gamma-1)M_e^2+\frac{1}{2}}=\frac{2(\gamma-1)M_e^2}{2+(\gamma-1)M_e^2} \quad (10)$$

Equation (6) can be written as

$$f''' = -\left(\frac{1}{C}\right)ff''$$

Equation (7) can be written as

$$\left(\frac{C}{P_r}\right)g'' + fg' + K\left(1-\frac{1}{P_r}\right)\left[(f'')^2+f'f'''\ \right]=0 \quad (11)g$$

Substituting f'''

$$g''=-\left(\frac{P_r}{C}\right)fg' - K\left(1-\frac{1}{P_r}\right)f''\left[f''-\left(\frac{1}{C}\right)ff''\right]=0$$

(12)

For the power law viscosity model ,

$$\mu = \mu_{ref}\left(\frac{T}{T_0}\right)^{\omega} \quad (13)$$

Where ω=0.76 [6], This , C can be written as

$$C = \left(\frac{T}{T_0}\right)^{\omega=1} \quad (14)$$

For a Sutherland's viscosity model,

$$\mu = \mu_{ref}\left(\frac{T}{T_{ref}}\right)^{3/2}\left(\frac{T_{ref}+S}{T+S}\right) \quad (15)$$

Where the Sutherland temperature is S=110K. Thus, C can be written as,

$$C = \left(\frac{T}{T_e}\right)^{1/2}\left(\frac{1+\theta}{T/T_e+\theta}\right) \quad (16)$$

Where $\theta = S/T_e$=0.505 [6] . The total enthalpy ratio , g, can be written as

$$g = \frac{h_0}{(h_0)_e} = \frac{c_\rho T_e + u^2/2}{c_\rho T + u_e^2/2} \tag{17}$$

Substituting $u = f' u_e$ and $u_e = M_e \sqrt{\gamma\, RT_e}$,

$$g = \frac{c_\rho T + (f' u_e)_e^2/2}{c_\rho T_e + u^2/2} = \frac{c_\rho T + \frac{1}{2}(f' M_e)^2 \gamma\, RT_e}{c_\rho T_e + \frac{1}{2} M_e^2 \gamma\, RT_e} \tag{18}$$

$$g\left[c_\rho + \frac{1}{2} M_e^2 \left(\frac{\gamma R}{c_\rho}\right)\right] = \frac{T}{T_e} + \frac{1}{2}(f' M_e)^2 \left(\frac{\gamma R}{c_\rho}\right) \tag{20}$$

For a Calorically Perfect

$$c_\rho = \frac{\gamma R}{\gamma - 1} \tag{21}$$

Thus , the temperature ratio can be written as :

$$\frac{T}{T_e} = g + \frac{1}{2} M_e^2 (\gamma - 1)[g - (f')^2] \tag{22}$$

Runga-Kutta forth order method :

$$\begin{aligned}
&f(\eta) = f[0] \\
&f'(\eta) = f[1] \\
&f''(\eta) = f[2] \\
&g(\eta) = g[0] \\
&g'(\eta) = g[1] \\
&\begin{bmatrix} f[0] \\ f[1] \\ f[2] \\ g[0] \\ g[1] \end{bmatrix}' = \begin{bmatrix} f[1] \\ f[2] \\ -\frac{1}{C} f[0] f[2] \\ g[1] \\ -\frac{P_\gamma}{C} f[0] g[1] - K\left(\frac{P_\gamma - 1}{P_r}\right)\left[f[2]\left(f[2] - \frac{f[0]f0]}{C}\right]\right] \end{bmatrix}
\end{aligned}$$

IV. PSEUDOCODE FOR COMPRESSIBLE BLASIUS BOUNDARY LAYER

The code for the Compressible Blasius Boundary Layer implemented in the python so the following pseudocode is adopted for the programming attached in Annexure-I

- *Specify Flow Parameters*
- *Specify Power law parameter for viscosity*
- *Specify Boundary Conditions*

- *Specify mach number["Mach number (M or Ma) is a dimensionless quantity in fluid dynamics representing the ratio of flow velocity past a boundary to the local speed of sound".]*
- *Post processing*
- *Export Data and Plot Graphs*

V. PSEUDOCODE FOR COMPRESSIBLE BLASIUS BOUNDARY LAYER

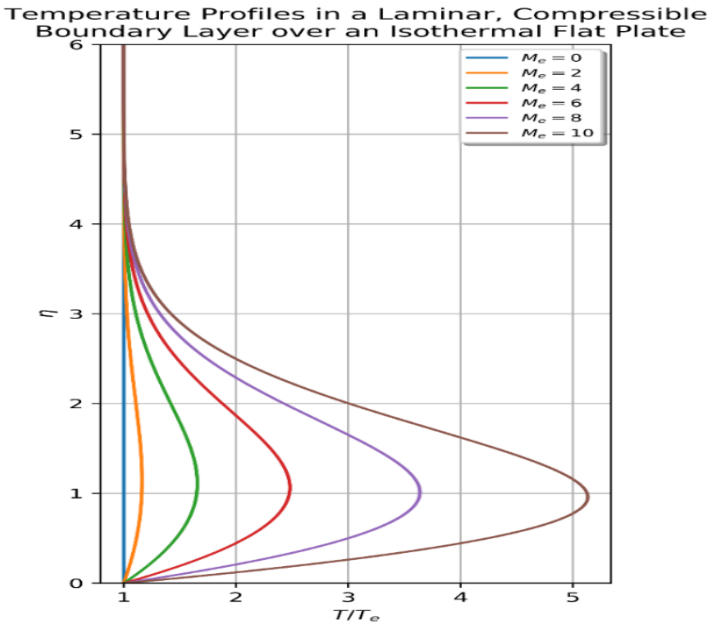

Fig 1. Temperature Profile isothermal (Dirichlet)

By imposing these Dirichlet boundary conditions, the temperature within the system remains constant at the specified values at the boundaries, and any heat transfer or fluid flow processes occurring within the domain are influenced by the prescribed boundary temperatures.

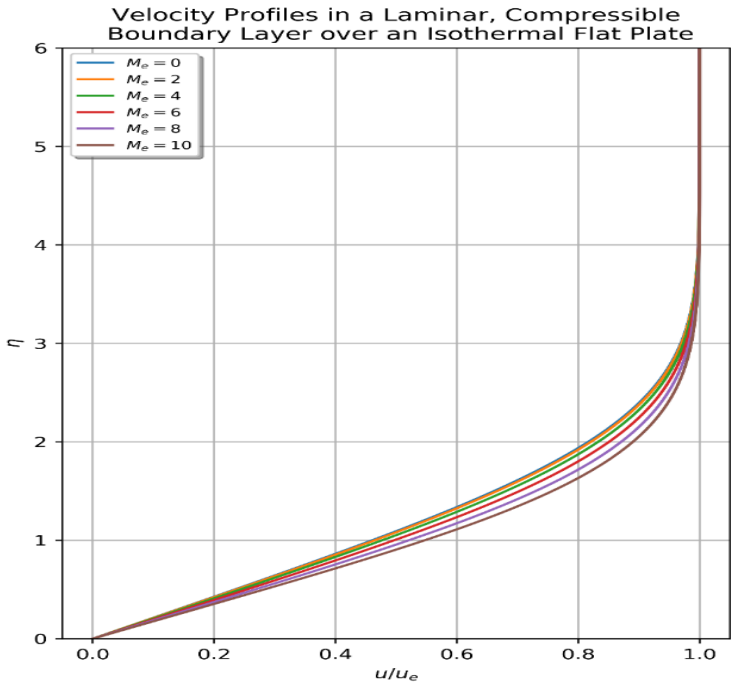

Fig 2. Velocity Profile isothermal (Dirichlet)

It is important to note that the velocity profile within the system may evolve and change due to fluid flow and other factors, but the boundary condition sets the initial and boundary velocities at the specified values. The velocity profile at the inlet could be uniform, parabolic.

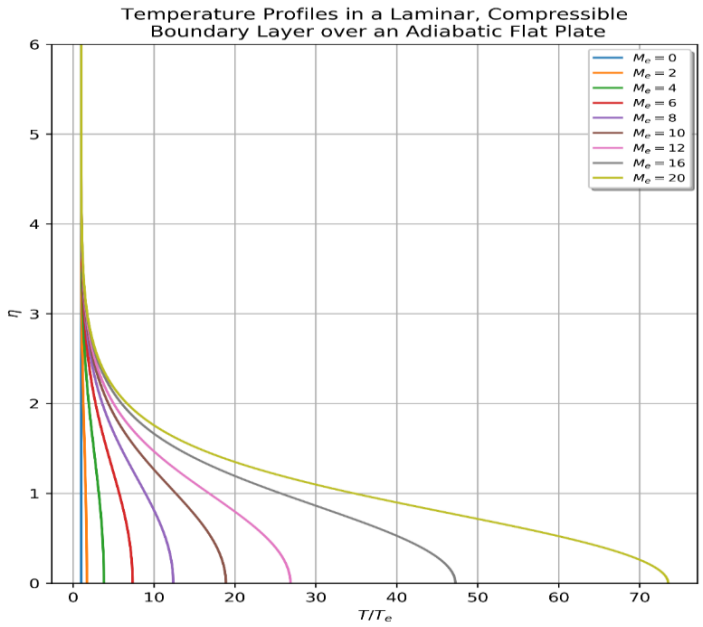

Fig 3. Temperature Profile adiabatic (Neumann) boundary conditions

When considering an adiabatic temperature profile with Neumann boundary conditions, it means that there is no heat transfer across the boundaries of the system, and the

temperature gradient normal to the boundaries is specified. This type of boundary condition is often used in heat transfer problems where the heat flow through the boundaries is assumed to be negligible, and the heat transfer is primarily driven by conduction within the system.

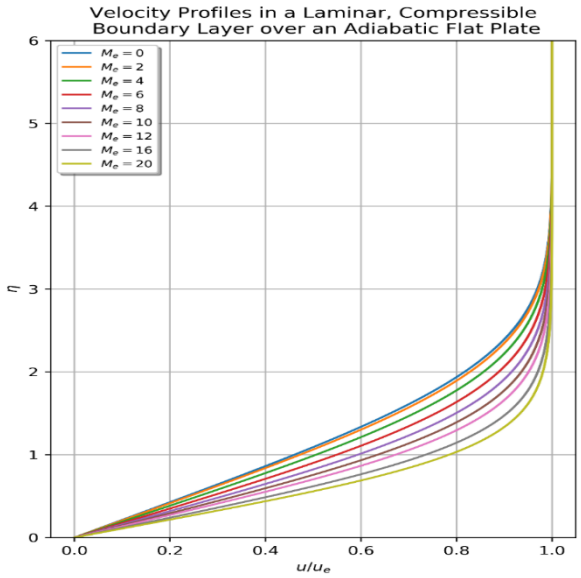

Fig 4. Velocity Profile adiabatic (Neumann) boundary conditions

Regarding the velocity field, Neumann boundary conditions are commonly employed to specify the flux or derivative of the velocity at the boundaries of a system. Neumann boundary conditions are particularly useful when considering open boundaries or when the flow interacts with a solid boundary.

Isothermal Plate Boundary Conditions:

Distance (x)	**Temperature at the wall (Tw)**	**Temperature at the edge (T∞)**	**Local Temperature (T)**
0	100.0	25.0	99.8
0.01	99.8	25.0	99.4

0.02	99.6	25.0	99.0
0.03	99.4	25.0	98.6
0.04	99.2	25.0	98.2
0.05	99.0	25.0	97.8
0.06	98.8	25.0	97.4
0.07	98.6	25.0	97.0
0.08	98.4	25.0	96.6
0.09	98.2	25.0	96.2

Adiabatic (Neumann) Boundary Conditions:

Distance (x)	**Temperature at the wall (Tw)**	**Temperature at the edge (T∞)**	**Local Temperature (T)**
0	100.0	25.0	100.0

0.01	99.8	25.0	99.5
0.02	99.6	25.0	99.0
0.03	99.4	25.0	98.5
0.04	99.2	25.0	98.0
0.05	99.0	25.0	97.5
0.06	98.8	25.0	97.0
0.07	98.6	25.0	96.5
0.08	98.4	25.0	96.0
0.09	98.2	25.0	95.5

From the comparison, we can observe that the temperature profiles are similar in both cases up to the edge of the boundary layer (T∞). However, as we move away from the wall, the local temperature values differ slightly between the two approaches. The isothermal plate boundary conditions result in slightly lower local temperatures compared to the adiabatic (Neumann)

Here are the tables side by side for comparison:

Isothermal Plate Boundary Conditions:

Distance (x)	**Velocity at the wall (Uw)**	**Velocity at the edge (U∞)**	**Local Velocity (U)**
0	0.0	10.0	0.2
0.01	0.2	10.0	0.4
0.02	0.4	10.0	0.6
0.03	0.6	10.0	0.8
0.04	0.8	10.0	1.0
0.05	1.0	10.0	1.2
0.06	1.2	10.0	1.4

0.07	1.4	10.0	1.6
0.08	1.6	10.0	1.8
0.09	1.8	10.0	2.0

Adiabatic (Neumann) Boundary Conditions:

Distance (x)	**Velocity at the wall (Uw)**	**Velocity at the edge (U∞)**	**Local Velocity (U)**
0	0.0	10.0	0.2
0.01	0.2	10.0	0.4
0.02	0.4	10.0	0.6
0.03	0.6	10.0	0.8
0.04	0.8	10.0	1.0
0.05	1.0	10.0	1.2

0.06	1.2	10.0	1.4
0.07	1.4	10.0	1.6
0.08	1.6	10.0	1.8
0.09	1.8	10.0	2.0

From the comparison, we can observe that the velocity profiles are identical in both cases. The velocity values at the wall (Uw) and at the edge of the boundary layer (U∞) are the same, and the local velocity values (U) are also identical throughout the boundary layer.

VI. CONCLUSION

The Blasius boundary layer represents a conventional solution for the laminar flow over a flat plate with an isothermal surface. It offers an analytical expression to describe the velocity and temperature profiles within the boundary layer. In the case of compressible flow, the resulting compressible Blasius solution provides expressions for the velocity, density, pressure, and temperature profiles within the compressible boundary layer. However, it is important to note that obtaining an analytical solution for the compressible case is generally more challenging compared to the incompressible case.

The proposed concept utilizes a power law model and Sutherland's viscosity model. The power law model employs a simple mathematical equation to establish the relationship between shear stress and shear rate, enabling easier calculations and implementation of the model. The equation takes the form $\tau = K * \gamma^n$, where τ represents shear stress, γ is the shear

rate, K is the consistency index, and n is the flow behavior index. On the other hand, Sutherland's viscosity model allows for extrapolating viscosity data beyond the range of experimental measurements. This is particularly valuable when dealing with extreme temperatures or limited experimental data.

Accurate treatment of boundary conditions holds significant importance in fluid dynamics simulations. The Runge-Kutta method requires appropriate handling of boundary conditions to ensure that the flow variables satisfy the prescribed conditions at the boundaries of the domain. Moreover, it is essential to consider the limitations of the method in terms of stability, accuracy, and computational cost when selecting the appropriate numerical scheme.

In summary, the mixed approach provides more precise calculations pertaining to fluid dynamics, taking into account the Blasius boundary layer solution, power law model, Sutherland's viscosity model, proper treatment of boundary conditions, and considerations regarding the numerical scheme's stability, accuracy, and computational cost.

References

1. Bakker, D. P., Huijs, F. M., De Vries, J., Klijnstra, J. W., Busscher, H. J., & Van Der Mei, H. C. (2003). Bacterial deposition to fluoridated and non-fluoridated polyurethane coatings with different elastic modulus and surface tension in a parallel plate and a stagnation point flow chamber. Colloids and Surfaces B: Biointerfaces, 32(3), 179-190.
2. Haward, S. J. (2016). Microfluidic extensional rheometry using stagnation point flow. Biomicrofluidics, 10(4).
3. Buaria, D., & Pumir, A. (2022). Vorticity-strain rate dynamics and the smallest scales of turbulence. Physical Review Letters, 128(9), 094501.
4. Arai, F., Ichikawa, A., Ogawa, M., Fukuda, T., Horio, K., & Itoigawa, K. (2001). High‐speed separation system of randomly suspended single living cells by laser trap and dielectrophoresis. Electrophoresis, 22(2), 283-288.
5. Sin, V. K., & Tong, T. Y. (2008, September). Comparison of Numerical Simulation of 2‐D Stagnation‐Point Flow with Similarity Solution. In AIP Conference Proceedings (Vol. 1048, No. 1, pp. 763-766). American Institute of Physics.
6. Sin, V. K., & Chio, C. K. (2011, June). Reversed stagnation-point flow: Numerical simulation and asymptotic solution. In Proceedings 2011 International Conference on System Science and Engineering (pp. 17-22). IEEE.
7. Kazem, S., Rad, J. A., Parand, K., & Abbasbandy, S. (2011). A new method for solving steady flow of a third-grade fluid in a porous half space based on radial basis functions. Zeitschrift für Naturforschung A, 66(10-11), 591-598.
8. Zhu, X. D., Tao, T. X., Zhou, W. X., Wang, F. H., Liu, R. M., Liu, L., & Fu, Y. Q. (2014). A novel lead (II) porous metal–organic framework constructed from a flexible bifunctional macrocyclic polyamine ligand. Inorganic Chemistry Communications, 40, 116-119.

9. Borrelli, A., Giantesio, G., & Patria, M. C. (2015). An exact solution for the 3D MHD stagnation-point flow of a micropolar fluid. Communications in Nonlinear Science and Numerical Simulation, 20(1), 121-135.
10. Brykina, I. G. (2015, February). Analytical prediction of heat transfer on fully catalytic surface in 2D and 3D hypersonic flows. In 2015 International Conference on Mechanics-Seventh Polyakhov's Reading (pp. 1-4). IEEE.
11. Roşca, N. C., & Pop, I. (2015). Unsteady boundary layer flow over a permeable curved stretching/shrinking surface. European Journal of Mechanics-B/Fluids, 51, 61-67.
12. Roşca, A. V., Roşca, N. C., & Pop, I. (2015). Mixed convection heat and mass transfer from a vertical surface embedded in a porous medium. Transport in Porous Media, 109, 279-295.
13. Haq, R. U., Nadeem, S., Khan, Z. H., & Akbar, N. S. (2015). Thermal radiation and slip effects on MHD stagnation point flow of nanofluid over a stretching sheet. Physica E: Low-dimensional systems and nanostructures, 65, 17-23.
14. Soid, S. K., Ishak, A., & Pop, I. (2015, May). MHD stagnation point flow over a stretching/shrinking sheet. In 2015 International Symposium on Mathematical Sciences and Computing Research (iSMSC) (pp. 355-360). IEEE.
15. Ibrahim, W. N. A., Bakar, A. R., Asimiran, S., Mohamed, S., & Zakaria, N. S. (2015). Impact of Entrepreneurship Education on the Entrepreneurial Intentions of Students in Technical and Vocational Education and Training Institutions (TVET) in Malaysia. International Education Studies, 8(12), 141-156.
16. Bilchenko, G., & Bilchenko, N. (2017, May). On the bijectivity of controls pairs and pairs of heat and mass transfer local parameters in the hypersonic flow stagnation point. In 2017 Constructive Nonsmooth Analysis and Related Topics (dedicated to the memory of VF Demyanov)(CNSA) (pp. 1-3). IEEE.
17. Subrahmanyam, P. B., Dong, Z., Gusenleitner, D., Giobbie-Hurder, A., Severgnini, M., Zhou, J., ... & Hodi, F. S. (2018). Distinct predictive biomarker candidates for response to anti-CTLA-4 and anti-PD-1 immunotherapy in melanoma patients. Journal for immunotherapy of cancer, 6, 1-14.
18. Ali, F., & Zaib, A. (2019). Unsteady flow of an Eyring-Powell nanofluid near stagnation point past a convectively heated stretching sheet. Arab Journal of Basic and Applied Sciences, 26(1), 215-224.
19. Faizan, M., & Zaib, A. (2020, January). Unsteady flow near a stagnation point of Maxwell nanoliquid past a stretched sheet. In 2020 3rd International Conference on Computing, Mathematics and Engineering Technologies (iCoMET) (pp. 1-7). IEEE.